

RESEARCH ARTICLE

10.1002/2013WR014785

Key Points:

- Resolution analysis was applied to tomographic slug tests head data
- Tomographic slug tests provide independent estimates of K_h , K_v/K_h , and S_s
- Head data can resolve coarse heterogeneities in hydraulic properties

Correspondence to:

D. Paradis,
dparadis@nrcan.gc.ca

Citation:

Paradis, D., E. Gloaguen, R. Lefebvre, and B. Giroux (2015), Resolution analysis of tomographic slug test head data: Two-dimensional radial case, *Water Resour. Res.*, 51, 2356–2376, doi:10.1002/2013WR014785.

Received 24 SEP 2013

Accepted 10 MAR 2015

Accepted article online 18 MAR 2015

Published online 11 APR 2015

Resolution analysis of tomographic slug test head data: Two-dimensional radial case

Daniel Paradis^{1,2}, Erwan Gloaguen², René Lefebvre², and Bernard Giroux²

¹Geological Survey of Canada, Quebec City, Canada, ²Institut national de la recherche scientifique, Centre Eau Terre Environnement, Quebec City, Canada

Abstract Hydraulic tomography inverse problems, which are solved to estimate aquifer hydraulic properties between wells, are known to be ill-conditioned and a priori information is often added to regularize numerical inversion of head data. Because both head data and a priori information have effects on the inversed solution, assessing the meaningful information contained in head data alone is required to ensure comprehensive interpretation of inverse solutions, whether they are regularized or not. This study thus aims to assess the amount of information contained in tomographic slug tests head data to resolve heterogeneity in K_h , K_v/K_h , and S_s . Therefore, a resolution analysis based on truncated singular value decomposition of the sensitivity matrix with a noise level representative of field measurements is applied using synthetic data reflecting a known littoral aquifer. As an approximation of the hydraulic behavior of a real aquifer system, synthetic tomographic experiments and associated sensitivity matrices are generated using a radial flow model accounting for wellbore storage to simulate slug tests in a plane encompassing a stressed well and an observation well. Although fine-scale resolution of heterogeneities is limited by the diffusive nature of the groundwater flow equations, inversion of tomographic slug tests head data holds the potential to uniquely resolve coarse-scale heterogeneity in K_h , K_v/K_h , and S_s , as inscribed in the resolution matrix. This implies that tomographic head data can provide key information on aquifer heterogeneity and anisotropy, but that fine-scale information must be supplied by a priori information to obtain finer details.

1. Introduction

It is widely recognized that knowledge of the spatial distribution of aquifer and aquitard hydraulic properties within an aquifer system is essential to the understanding of its dynamics, which provides the basis for sound groundwater management. Indeed, comprehensive aquifer characterization should ideally rely on a three-dimensional model of the architecture of the aquifer system units and their respective hydraulic properties [e.g., Anderson, 1989; Ouillon *et al.*, 2008; Bayer *et al.*, 2011; Chen *et al.*, 2012; Di Maio *et al.*, 2014]. Hydraulic tomography, which is essentially the simultaneous analysis of multiple interwell hydraulic tests, such as pumping [e.g., Tosaka *et al.*, 1993; Gottlieb and Dietrich, 1995; Butler *et al.*, 1999; Yeh and Liu, 2000; Bohling *et al.*, 2002, 2007; Zhu and Yeh, 2005; Illman *et al.*, 2007, 2008; Fienen *et al.*, 2008; Cardiff *et al.*, 2009; Illman *et al.*, 2009; Berg and Illman, 2011, 2013, 2015; Cardiff and Barrash, 2011; Huang *et al.*, 2011; Cardiff *et al.*, 2012; Sun *et al.*, 2013] and slug tests [e.g., Brauchler *et al.*, 2003], is increasingly recognized as a promising technique for imaging heterogeneity in hydraulic properties at local scale, which can lead to preferential flow paths or impermeable barriers that control flow and transport in aquifers. Cardiff and Barrash [2011] provided a comprehensive review of studies on hydraulic tomography.

In hydraulic tomography, multiple hydraulic head responses measured in stressed and observation intervals are inverted to estimate the spatial heterogeneity in hydraulic properties between two or more wells, such as hydraulic conductivity (K) and specific storage (S_s). Tomographic inverse problems are generally ill-conditioned, sometimes even rank-deficient, as the number of unknown model parameters is usually greater than the number of available head data [Carrera and Neuman, 1986; Tonkin and Doherty, 2005]. Resulting overparameterized solutions are thus nonunique [Bohling, 2009; Bohling and Butler, 2010], especially under real field conditions where noise in the head data limits parameter resolution [e.g., Yeh and Liu, 2000; Illman *et al.*, 2008; Xiang *et al.*, 2009; Huang *et al.*, 2011; Liu and Kitanidis, 2011], as small head variations caused by geological heterogeneities can be hindered by noisy head data.

A class of solution of the Gaussian linear inverse problem that is applicable in hydraulic tomography is the generalized inverse [Menke, 2012]. Generalized inverse solutions can be viewed in two different ways: either as a point estimate, or localized average of model parameters. First, when the solution is viewed as point estimate, each parameter of the solution can be considered as unique only if we accept as appropriate the a priori information used to supplement head data [Bohling and Butler, 2010]. Different strategies to integrate a priori information have been proposed to converge to a unique solution with hydraulic tomographic problems, such as the use of objective function terms that penalize deviations from an a priori covariance [e.g., Carrera and Neuman, 1986; Kitaniadis, 1995; Yeh and Liu, 2000; Fienen et al., 2008; Illman et al., 2008; Berg and Illman, 2011; Cardiff and Barrash, 2011; Huang et al., 2011; Cardiff et al., 2012; Sun et al., 2013] or the addition of smoothing, flatness, robust constraints [e.g., Tikhonov, 1963; Tikhonov and Arsenin, 1977; Doherty, 2003; Tonkin and Doherty, 2005]. Conditioning parameter estimates coming from indirect measurements of hydraulic properties [Carrera et al., 2005; Illman et al., 2008], groundwater fluxes [Zha et al., 2014], environmental tracers [Vasco et al., 1997], or correlated geophysical properties [e.g., Rubin and Hubbard, 2005; Caers, 2005; Soueid Ahmed et al., 2014] have been also proposed. In most instances, the choice of a priori information should be carefully considered since inappropriate use of this complementary information to head data induce important bias in hydraulic property estimates [Illman et al., 2008; Cardiff and Barrash, 2011]. Second, when the same inverse solution is interpreted as a localized average, the solution can be viewed as a unique quantity that exists independently of any a priori information applied to the inverse problem. Examination of the sensitivity matrix for a given tomographic experiment through a resolution analysis may indeed reveal the averaging properties of the inverse solution [e.g., Vasco et al., 1997; Day-Lewis et al., 2005]. That is, parameters that cannot be resolved independently can be identified and used together to remove nonuniqueness. The required cost and effort needed to obtain meaningful a priori information for fine-scale estimates of hydraulic properties may not be justified in some practical applications. Thus, the characterization of coarse-scale heterogeneity in hydraulic properties, provided by averaging tomographic inverse solution based on head data, could represent an efficient aquifer characterization alternative. As such, tomographic head data by themselves can yield, at the very least, key preliminary information on aquifer heterogeneities that may be subsequently targeted for more detailed and costly investigations by adding data to be used as a priori information for inversion.

In this paper, tomographic slug tests head data are used to estimate coarse-scale heterogeneity in horizontal hydraulic conductivity (K_h), K anisotropy (ratio of vertical and horizontal K , K_v/K_h), and specific storage S_s . The scientific objective is to assess the spatial information on hydraulic properties that can be obtained solely from the analysis of tomographic head data, as this knowledge could be used to better design hydraulic tests for tomographic experiments and eventually better understand the characteristics of the a priori information that should be gathered to complement head data to provide fine-scale estimates of hydraulic parameters.

In this paper, we present the analysis of tomographic slug tests head data in the plane encompassed by a stressed well and an observation well. The head data are obtained from a series of synthetic tomographic slug tests experiments represented by a 2-D radial numerical flow model. This approach allows the investigation of the effect of various factors influencing the resolution of K_h , K_v/K_h , and S_s . In particular, we investigate measurement error, experimental design, magnitude in hydraulic property values, spatial structure of the hydraulic properties, and discretization. The resolution analysis is based on truncated singular value decomposition of the sensitivity matrix for a predetermined level of relative parameter error [e.g., Clemo et al., 2003; Bohling, 2009]. Synthetic scenarios reflect the general aquifer characteristics and experimental configuration of a field implementation of tomographic slug tests in a littoral aquifer reported by Paradis [2014] and Paradis et al. [2014]. Laboratory and field tests for this aquifer indicate significant differences in K_h and K_v values over intervals smaller than the length of the stressed intervals used for the field implementation of tomographic slug tests [Paradis and Lefebvre, 2013]. Thus, for the purpose of the synthetic tomographic experiments, we assume that the numerical model representing flow through this aquifer cannot be described using isotropic K values, and that fine-scale K anisotropy can be captured using K_v/K_h values at the scale of the parameter grid cells. On the other hand, resolving the heterogeneous structure of the aquifer can capture coarse-scale K anisotropy effects. Finally, while tomographic slug tests have been extensively studied using the concept of hydraulic travel time [Brauchler et al., 2007, 2010 and 2011; Hu et al., 2011] to estimate heterogeneity in hydraulic diffusivity (the ratio K/S_s), their resolution potential to individually assess heterogeneity in K_h , K_v/K_h , and S_s as demonstrated in this study has never been assessed.

2. Approach

In this section, we present the forward radial flow model used to simulate synthetic tomographic experiments and to derive the corresponding sensitivity matrix. Then, we explain the approach used to evaluate a Moore-Penrose pseudoinverse [Moore, 1920; Penrose, 1955] based on truncated singular value decomposition (SVD) of the sensitivity matrix from which is derived a resolution matrix. The analysis of the resolution matrix will serve in the next section to assess the resolution potential of tomographic slug test head data when solving the inverse problem for different synthetic experiments.

2.1. Forward Modeling

For this study, synthetic tomographic experiments were simulated using the Ir2dinv numerical simulator [Bohling and Butler, 2001], a two-dimensional radial-vertical finite-difference groundwater flow model. Under conditions of radial symmetry, implying the absence of angular variations in both hydraulic properties and boundary conditions, the flow to a partially penetrating stressed interval in response to an instantaneous change in water level in a confined aquifer of infinite areal extent may be described using the radial groundwater flow equation:

$$\frac{1}{r} \frac{\partial}{\partial r} \left(r K_r \frac{\partial h}{\partial r} \right) + \frac{\partial}{\partial z} \left(K_z \frac{\partial h}{\partial z} \right) = S_s \frac{\partial h}{\partial t} \quad (1)$$

where h is the head (L), S_s is the specific storage (1/L), K_r and K_z are, respectively, the hydraulic conductivity in the radial (or horizontal- K_h) and vertical directions, t is time (T), r is the radial coordinate (L), and z is the vertical coordinate (positive downward from a zero reference at the top of the aquifer) (L).

The inner boundary of the model is at the stressed well radius r_w (L) and the initial conditions are given as follows:

$$h(r, z, 0) = 0 \quad r_w < r < r_m \quad 0 < z < b \quad (2)$$

$$H(0) = H_0 \quad (3)$$

where r_m is the outer boundary of the model located far away from the stressed well in order not to interfere with it, b (L) is aquifer thickness, H is level of water in the well (L), and H_0 is the static water column height in the well where the stressed interval is located, which is equal to the initial level of water in the well at $t=0$, (L).

The outer boundary conditions are the following:

$$h(r=r_m, z, t) = 0 \quad t > 0 \quad 0 \leq z \leq b \quad (4)$$

$$\frac{\partial h(r, 0, t)}{\partial z} = \frac{\partial h(r, b, t)}{\partial z} = 0 \quad t > 0 \quad r_w < r < r_m \quad (5)$$

and the inner boundary conditions at the stressed interval is given by

$$\frac{1}{L} \int_{d-L}^d h(r_w, z, t) dz = H(t) \quad t > 0 \quad (6)$$

$$2\pi r_w K_r \frac{\partial h(r_w, z, t)}{\partial r} = \begin{cases} 0 & z < d-L, z > d \quad t > 0 \\ \frac{\pi r_c^2}{L} \frac{dH(t)}{dt} & d-L \leq z \leq d \quad t > 0 \end{cases} \quad (7)$$

where d is the distance from the top of the aquifer to the bottom of the stressed interval (L), L is the stressed screen length (L), and r_c is the radius of well casing (L).

To explicitly simulate wellbore storage effects and placement of packer intervals in the well, one column of cells is used to represent the region inside the wellbore, from the wellbore radius, r_w , to the inner radius of the model grid, r_{min} . Wellbore processes are approximated using a Darcy's Law formulation, with open sections of the wellbore (stressed intervals) represented as high- K regions ($K_h = 1 \times 10^5$ m/s, $K_v = 1 \times 10^8$ m/s)

and packers as low- K regions ($K_h=K_v=1 \times 10^{-12}$ m/s). Cells in the wellbore are also assigned a value of S_s equal to 0, representing the fact that water is essentially incompressible, except for the top cell of the stressed interval for which a S_s value of 1 is assigned and converted to the following value:

$$S_s = \frac{1}{\Delta z} \left(\frac{r_c^2}{r_w^2 - r_{min}^2} \right) \quad (8)$$

This value accounts for the vertical thickness of the cell, Δz , and compensates for the exclusion of the inner portion of the wellbore (between $r=0$ and $r=r_{min}$) from the radial model domain. r_c is the radius of the well casing above the wellbore screen radius, r_w .

Note that the simulation of wellbore storage effects is a key factor to be considered for tomographic slug tests interpretation [Prats and Scott, 1975; Spang, 1996; Brauchler et al., 2007; Paradis and Lefebvre, 2013]. In fact, large wellbore storage (i.e., $r_c > r_w$) for a stressed interval delays and lengthens the head perturbation induced into an aquifer, as the change in head in the wellbore is slower due to the larger radius of the well casing, r_c , with respect to the wellbore screen radius, r_w . Large wellbore storage also amplifies the head response in an observation interval because more water is used to carry out the test. While observation interval response is sensitive to wellbore storage, wellbore storage makes the estimation of S_s from stressed interval response more difficult when the volume of stored water in the wellbore is much larger than the storage capacity of the aquifer [Cooper et al., 1967]. That is, stressed interval response is rather insensitive to change in S_s value in this case. Thus, explicit modeling of wellbore storage will result in better estimation of hydraulic properties. Note that for the synthetic simulations we neglected wellbore storage effects in the observation intervals because we assume that each observation interval is straddled with packers to avoid storage effects [Sageev, 1986]. To simulate slug tests, the initial head in the top cell of the open section of the wellbore is set to the initial displacement for the test, H_0 , with all other initial heads in the model set to zero. For modeling radial flow induced by a slug test, the model uses a logarithmic transform of the radial coordinate to transform the radial flow problem into an equivalent problem in Cartesian coordinates. Details about the transform and solving of the resulting Cartesian flow equation with transformed values using block-centered finite-difference formulation are found in Butler and McElwee [1995] and Bohling and Butler [2001].

2.2. Sensitivity Calculation

The sensitivity relates a change in a parameter to a corresponding change in the heads. For this study, each $J_{m,n}$ element in the sensitivity matrix represents the normalized sensitivity of the head at a given time and location, h_m , to one of the model parameter, p_n :

$$J_{m,n} = p_n \frac{\partial h_m}{\partial p_n} \quad (9)$$

The head index m runs over all observation times and locations for all simulated tests, and p_n represents either the K_h , K_v/K_h , or S_s value associated with each of the cells in the parameter grid used for the numerical simulation. This normalization brings the sensitivities of the different parameters to an equal level for a change of head in response to a unit relative change in the parameter value. Differences in magnitude in the relative sensitivities are thus more indicative of the actual relative influence of each parameter [Bohling and Butler, 2001]. Notice that the sensitivity matrix here represents a linear approximation of the nonlinear behavior of the flow nearby the parameters used in the synthetic simulations, which is a fair approximation to evaluate the resolution potential of mild nonlinear problems such as the groundwater flow problem represented by (1) [Vasco et al., 1997]. In this work, the sensitivity matrix elements are constructed by a sequence of groundwater flow simulations using Ir2div, one simulation per parameter grid cell, in which each hydraulic property in a single cell is slightly perturbed from its original value and the differences in head are noted.

2.3. Moore-Penrose Pseudoinverse

Consider a vector \mathbf{m} of n model parameters that we wish to estimate from a data vector, \mathbf{d} , of m observations. The inverse problem can thus be written as a linear system of equations [Aster et al., 2005]:

$$\mathbf{m} = \mathbf{J}\mathbf{d} \quad (10)$$

where \mathbf{J} is a $m \times n$ sensitivity matrix, as described in (9), that can be decomposed into its singular values, such as:

$$\mathbf{J} = \mathbf{U}\mathbf{S}\mathbf{V}^T \quad (11)$$

where \mathbf{U} is a $m \times m$ orthogonal matrix with columns that are unit basis vectors spanning the data space, \mathbb{R}^m . \mathbf{V} is a $n \times n$ orthogonal matrix with columns that are unit basis vectors spanning the model space, \mathbb{R}^n . \mathbf{S} is a $m \times n$ diagonal matrix with nonnegative diagonal singular values of \mathbf{J} . The singular values along the diagonal of \mathbf{S} are arranged in order of decreasing magnitude, and the columns of \mathbf{U} and \mathbf{V} are arranged in the corresponding order. The columns of \mathbf{V} represent linear combinations of the model parameters, and the leading columns, corresponding with the largest singular values, represent the linear combinations that are most strongly resolved by the data.

A singular value decomposition (SVD) analysis can be used to investigate the condition of an inverse problem and its noise amplification behavior, and it can also be used to compute a generalized inverse of \mathbf{J} , called the Moore-Penrose pseudoinverse, which is given by [Aster *et al.*, 2005]:

$$\mathbf{J}^\dagger = \mathbf{V}_p \mathbf{S}_p^{-1} \mathbf{U}_p^T \quad (12)$$

where only the p largest singular values and vectors, that correspond to the most strongly resolved parameters, have been retained. This pseudoinverse can then be used in computing estimated parameters, \mathbf{m}_\dagger , from observed data, \mathbf{d} , as

$$\mathbf{m}_\dagger = \mathbf{J}^\dagger \mathbf{d} \quad (13)$$

where \mathbf{m}_\dagger is a least squares and minimum length solution, regardless of the relative sizes of the rank of \mathbf{J} , m and n .

2.4. Resolution Matrix

To visualize the quality of the spatial coverage provided by a given tomographic experiment and to quantify the nonuniqueness of the inverse solution, we compute its resolution matrix, \mathbf{R} . If the true model is represented by \mathbf{m} and the corresponding true data vector is represented by $\mathbf{d} = \mathbf{J}\mathbf{m}$, then the estimated model parameter vector, \mathbf{m}_\dagger , can be expressed from (13) as [Aster *et al.*, 2005]:

$$\mathbf{m}_\dagger = \mathbf{J}^\dagger \mathbf{J}\mathbf{m} \quad (14)$$

The matrix multiplying the true model is the model parameter resolution matrix:

$$\mathbf{R} = \mathbf{J}^\dagger \mathbf{J} \quad (15)$$

where the elements of matrix \mathbf{R} are the averaging coefficients or the filter through which we view the hydraulic property structures resulting from the inversion [Vasco *et al.*, 1997]. For instance, R_{ij} denotes the contribution of the j th parameter to the estimate of the i th parameter. The resolution matrix is an array whose diagonal elements correspond to each grid cell of the model domain. The values of diagonal elements ($i=j$) are between 0 and 1. A value of 0 means that a given parameter cannot be resolved using the available observation data, and a value of 1 means it can be resolved perfectly. The off-diagonal elements ($i \neq j$) reflect the correlation of other elements on resolving the elements on the diagonal. Thus a value of zero in all the j th (j not equal to i) elements means that the parameter in the j th element has no effect on determining the i th element and, consequently, no spatial averaging would be present in the estimate.

For consistency among the comparison of the different synthetic tomographic experiments, we define the noise amplification behavior associated with each tomographic experiment and select individual number of p singular values and vectors to use in (15) to evaluate the pseudoinverse \mathbf{J}^\dagger of each experiment using a common level of model parameter error resulting from the inversion. As tomographic inverse problems are nonlinear and solved in a number of steps with the sensitivity matrix used as a linear approximation of the nonlinear flow at each step, the vector \mathbf{d} in (12) represents the matrix of residuals between the observed head data and corresponding simulated values at the current step, while \mathbf{m} represents a vector of parameter updates. Moreover, because the sensitivities in the sensitivity matrix are normalized, \mathbf{m} can be taken as a

Table 1. Synthetic Simulation Parameters and Average Resolution for Hydraulic Properties Within the Interwell Region (IWR) for Different Scenarios Assessing the Effects of the Signal-to-Noise Ratio, Tomographic Test Configuration, Magnitude of the Hydraulic Property Values and Discretization^a

Scenario	Model (K_h (ms^{-1})- K_v/K_h (-)- S_s (m^{-1}))	Grid Cells	Noise SD (m)	Initial Head (m)	Number of tx-rx	Unknowns/Rank	Condition Number	Singular Values Retained (p)	Average Resolution Within IWR (-)		
									K_h	K_v/K_h	S_s
1-Base case	1×10^{-5} - 0.1 - 1×10^{-5}	143	2×10^{-4}	4.5	13-37	429/429	6×10^{10}	136	0.57	0.30	0.48
2-Noise-free	1×10^{-5} - 0.1 - 1×10^{-5}	143	2×10^{-8}	4.5	13-37	429/429	5×10^{10}	366	0.99	0.99	1.00
3-Initial head	1×10^{-5} - 0.1 - 1×10^{-5}	143	2×10^{-4}	2.25	13-37	429/429	7×10^{10}	123	0.51	0.24	0.36
4-Initial head	1×10^{-5} - 0.1 - 1×10^{-5}	143	2×10^{-4}	9.0	13-37	429/429	7×10^{10}	143	0.60	0.36	0.52
5-Test configuration	1×10^{-5} - 0.1 - 1×10^{-5}	143	2×10^{-4}	4.5	13-59^b	429/429	5×10^{10}	142	0.62	0.36	0.51
6-Test configuration	1×10^{-5} - 0.1 - 1×10^{-5}	143	2×10^{-4}	4.5	13-48^c	429/429	5×10^{10}	156	0.65	0.47	0.54
7-Test configuration	1×10^{-5} - 0.1 - 1×10^{-5}	143	2×10^{-4}	4.5	26-74^d	429/429	4×10^{10}	223	0.92	0.63	0.71
8-Property magnitude	1×10^{-6} - 0.1 - 1×10^{-5}	143	2×10^{-4}	4.5	13-37	429/429	4×10^{10}	161	0.64	0.44	0.58
9-Property magnitude	1×10^{-4} - 0.1 - 1×10^{-5}	143	2×10^{-4}	4.5	13-37	429/424	5×10^{10}	105	0.51	0.25	0.39
10-Property magnitude	1×10^{-5} - 1 - 1×10^{-5}	143	2×10^{-4}	4.5	13-37	429/424	6×10^{10}	79	0.38	0.19	0.27
11-Property magnitude	1×10^{-5} - 0.01 - 1×10^{-5}	143	2×10^{-4}	4.5	13-37	429/429	3×10^{10}	190	0.66	0.31	0.64
12-Property magnitude	1×10^{-5} - 0.1 - 10^{-6}	143	2×10^{-4}	4.5	13-37	429/429	8×10^{10}	106	0.53	0.28	0.32
13-Property magnitude	1×10^{-5} - 0.1 - 10^{-4}	143	2×10^{-4}	4.5	13-37	429/429	1×10^{11}	149	0.63	0.33	0.61
14-Discretization	Heterogenous and anisotropic^f	143	2×10^{-4}	4.5	13-70	429/429	6×10^{10}	202	0.73	0.56	0.69
15-Discretization	Heterogenous and anisotropic^f	65	2×10^{-4}	4.5	13-70	195/195	2×10^{10}	156	0.98	0.92	0.92
16-Relative property magnitude	Heterogenous and anisotropic^f	65	2×10^{-4}	4.5	13-70^e	195/195	5×10^8	169	0.99	0.95	0.95

^aUnderlined text indicates modified parameter with respect to the base case scenario. Condition number values indicate moderated ill-conditioned inverse problems and unknown parameters greater than the matrix rank indicates rank deficient problems. SD stands for standard deviation. tx and rx stand for stressed (transmitter) and observation (receiver) intervals, respectively.

^b22 observation intervals added in the observation well.

^c11 observation intervals added in the stressed well.

^dReciprocal tests of the base case added.

^eStressed and observation wells inverted.

^fHeterogeneous and anisotropic hydraulic properties (see text).

vector of relative parameter updates [Clemo et al., 2003; Bohling, 2009]. Thus, with \mathbf{d} in (13) taken to represent the random noise in head data, η , \mathbf{m} can be interpreted as the error in the model parameters, $\Delta\mathbf{m}_+$, resulting from the noise in the data, as follows:

$$\Delta\mathbf{m}_+ = \mathbf{m} - \mathbf{m}_+ = \mathbf{J}^\dagger \eta \tag{16}$$

where \mathbf{m} is the true model as defined in (10) and the norm of $\Delta\mathbf{m}_+$ is a measure of the noise amplification error [Vogel, 2002]. Then, for a given level of model parameter error, defined here as the root mean square of the norm of $\Delta\mathbf{m}_+$, the number of p singular values and vectors to retain in the pseudoinverse of a given tomographic experiment can be selected to compute the associated resolution matrix [Bohling, 2009]. It has to be noted that as the number of p singular values and vectors retained in the pseudoinverse increase, model parameter error also increases to compensate for the increasing demand of resolution for less sensitive and highly correlated parameters associated with smaller singular values. A trade-off between apparent resolution and variance in the model parameter error should thus be generally achieved when solving the inverse problem.

3. Synthetic Experiments

In this section, we discuss a series of synthetic tomographic experiments (Table 1) that investigate the effect of factors that impact the resolution of hydraulic properties resulting from the analysis of tomographic slug tests head data. Specifically, we investigate measurement error, experimental design, magnitude in hydraulic property values, spatial structure of the hydraulic properties, and discretization. Results for various scenarios are compared with a base case example that reflects the general aquifer characteristics and experimental configuration of a field implementation of tomographic slug tests reported by Paradis [2014]. The present paper does not aim to exactly reproduce the test configuration or the hydraulic property fields themselves, but instead use similar test design and physical property values as the basis for various synthetic experiments to assess the information content of a transient analysis of tomographic slug tests.

The surficial sediments of the study area where tomographic slug tests have been carried out by *Paradis* [2014] consist primarily of Late Quaternary sandy and silty sediments that were deposited in the receding Champlain Sea, which was an arm of the Atlantic Ocean that had invaded the St. Lawrence Valley at the time of the last deglaciation [*Bolduc*, 2003; *Paradis et al.*, 2014; *Tremblay et al.*, 2014]. This littoral and sublittoral depositional environment resulted in superposition of long (>100 m) interdigitized sand and silt strata with fine vertical and lateral intrastratal transitions in grain size as a result of changing energy levels along Champlain Sea shorelines [*Paradis et al.*, 2014]. At the tomography site, values of K_h , based on multilevel slug tests in wells done at 15 cm intervals ranged from 7×10^{-7} to 2×10^{-5} m/s using the *Bouwer and Rice* [1976] method [*Paradis et al.*, 2011], whereas K_v estimates from permeameter tests on sediment samples at the same scale ranged from 2.7×10^{-8} to 1.0×10^{-5} m/s [*Paradis and Lefebvre*, 2013]. The comparison of K_h and K_v values for the same 15 cm intervals provides estimates of K_v/K_h , between 0.0025 and 0.83 as a result of the fine stratification of sand and silt sediments. Moreover, considering the results of the inversion of vertical interference slug test data, S_s values are shown to decrease with overburden thickness and vary from approximately 1×10^{-4} to 1×10^{-6} m⁻¹ [*Paradis and Lefebvre*, 2013]. The tomography field experiment involved a series of slug tests performed sequentially within 0.61 m long stressed intervals straddled by packers along fully screened direct-push wells separated by a distance of 7.98 m. During the slug tests, head responses were recorded with pressure transducers within the stressed interval and also within 0.30 m long observation intervals straddled by packers within an observation well and below the stressed interval.

For all synthetic experiments, we used a radial flow model to simulate stressed and observation interval responses in the plane encompassed by the stressed and observation wells, the interwell region (IWR). The model used a simulation grid with 43 cells of logarithmically increasing dimension along the radial axis and 26 cells of dimension 0.3048 m (1 foot) along the vertical axis (Figure 1a). Radial cell sizes are smaller near the stressed well, where hydraulic gradients induced by slug tests are larger. The scale of the logarithmic transform was adjusted to fit the radial location of the simulation grid nodes to the location of the wells with a well spacing identical to the field implementation. This discretization places the zero-head outer boundary of the model about 111 m from the stressed well, so that this boundary has negligible effects on simulated slug test heads at the stressed and observation wells. Confined conditions are also assumed for lower and upper boundary conditions.

Although we used a radial flow model with finer grid discretization near the stressed well to accurately represent larger hydraulic gradients near the stressed intervals, we used a different parameter grid with similar cell sizes to compare parameter sensitivities and resolutions on a common basis [e.g., *Bohling*, 2009]. The simulation grid was then divided into 143 cells of 0.61 m in height that corresponds to the length of the stressed interval (Figure 1b). Given the logarithmic change in cell dimensions in the radial direction, the cells of the simulation grid were merged laterally to obtain cell widths of approximately equal size within the IWR. The average width of the cells within the ROI is 1.46 m, which means that six columns of cells separate the stressed and observation wells. This 143 cell parameter grid was used for all synthetic simulations, except for discussion about discretization later on.

In order to provide a realistic estimate of parameter resolution under realistic field conditions, we added a Gaussian random noise with a mean of zero and a standard deviation of 2×10^{-4} m to actual synthetic head data. This noise level was evaluated from a residual analysis of head data recorded during the field implementation of the tomographic slug tests reported by *Paradis* [2014]. This noise level is consistent with observations by *Bohling* [2009] using tomographic pumping test data. Also, the resolution matrix for each synthetic experiment is computed using the number of p singular values and vectors (different for each experiment) that amplify the estimated random noise with a standard deviation of 2×10^{-4} m into mean square value of 0.01 for the norm of $\Delta \mathbf{m}$: (average relative model parameter error of 10%), thus providing a common basis of comparison for all synthetic experiments.

Finally, for all synthetic experiments, both stressed and observation interval responses are used in the computation of the respective sensitivity and resolution matrices. Indeed, temporal sensitivity curves for stressed and observation intervals are fairly different [*McElwee et al.*, 1995] and the combined use of all available head records can reduce sensitivity correlation between parameters, which is essential to maximize the resolution potential of tomographic experiments.

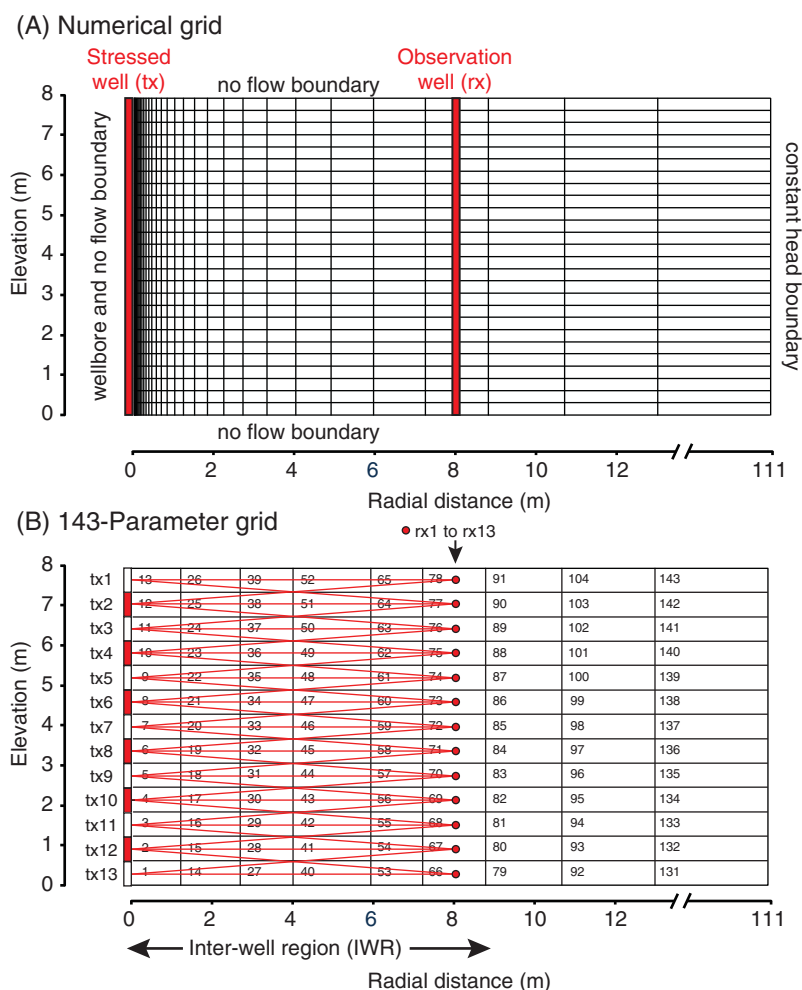


Figure 1. (a) Numerical grid and boundary conditions used for all synthetic tomographic experiments. (b) Parameter grid with 143 cells and zonation used for scenarios 1 through 14 (Table 1). Locations of stressed and observation intervals are also depicted in Figure 1b with red plain lines indicating associated intervals for each slug test where head data were used simultaneously for the base case scenario.

3.1. Spatial Sensitivity and Resolution of a Tomographic Experiment: Base Case

This section examines spatial sensitivity and resolution associated with a transient analysis of tomographic slug tests head data using a base case scenario. For the base case scenario, a homogeneous and anisotropic model with bulk average K_h , K_v/K_h , and S_s values of 1×10^{-5} m/s, 0.1, and $1 \times 10^{-5} \text{ m}^{-1}$, respectively, is used to simulate a tomographic experiment with 13 slug tests. Slug tests are carried out along a 8 m stressed well with simultaneous recording of heads in the stressed interval and three observation intervals (except for the upper and lower most stressed intervals that use two observation intervals) distributed along an observation well of identical length to provide relatively uniform spatial coverage of the IWR (Figure 1b). A total of 13 stressed and 37 observation interval responses are thus available for the base case analysis, which is considered a moderate coverage configuration that might be obtained in the field in only a few days. Although aquifers are inherently heterogeneous in nature, using a homogeneous model permits to isolate its effects from the effects of the various factors that influence resolution, in particular those from the effects of the spatial structure of hydraulic properties. Effects of the spatial structure of hydraulic properties will be discussed later in this paper.

3.1.1. Spatial Sensitivities

The resolution potential of tomographic slug tests data is first shown in Figure 2a which presents the RMS normalized sensitivity of heads to K_h , K_v/K_h , and S_s for the 13 slug tests using 13 stressed and 37 observation intervals (base case) in each cell of the parameter grid for a 10,000 s time frame. The RMS normalized sensitivity to K_h for parameter grid cell j is given by:

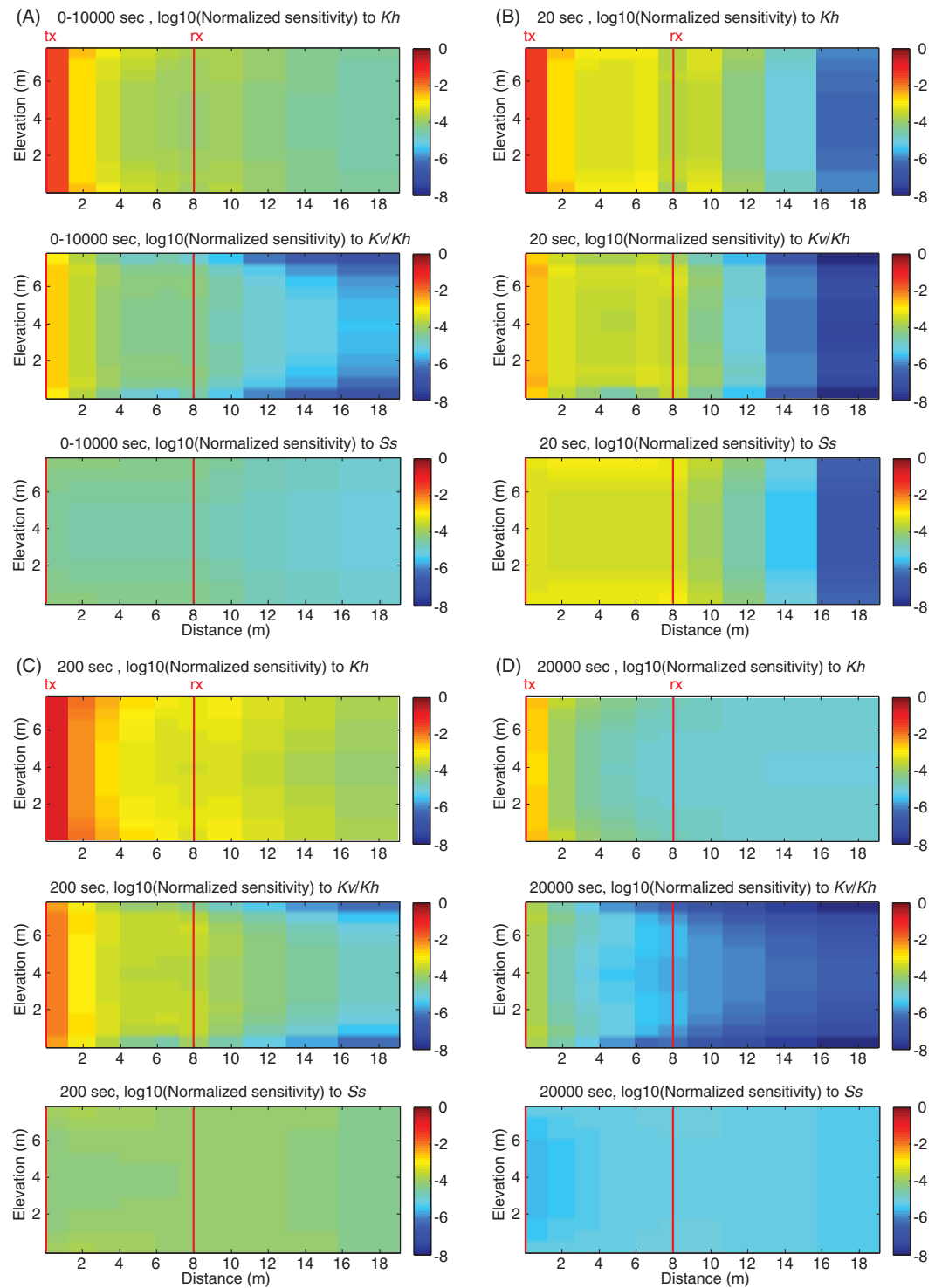


Figure 2. Spatial distributions of root mean square (RMS) normalized sensitivity to K_h , K_v/K_h , and S_s associated with the analysis of the synthetic 10,000 s head records for the base case scenario using an homogeneous and anisotropic model for different times: (a) time-integrated from 0 to 10,000 s; (b) for early time 20 s; (c) at approximately peak head amplitude in the observation intervals 200 s; and (d) at late time 2000 s.

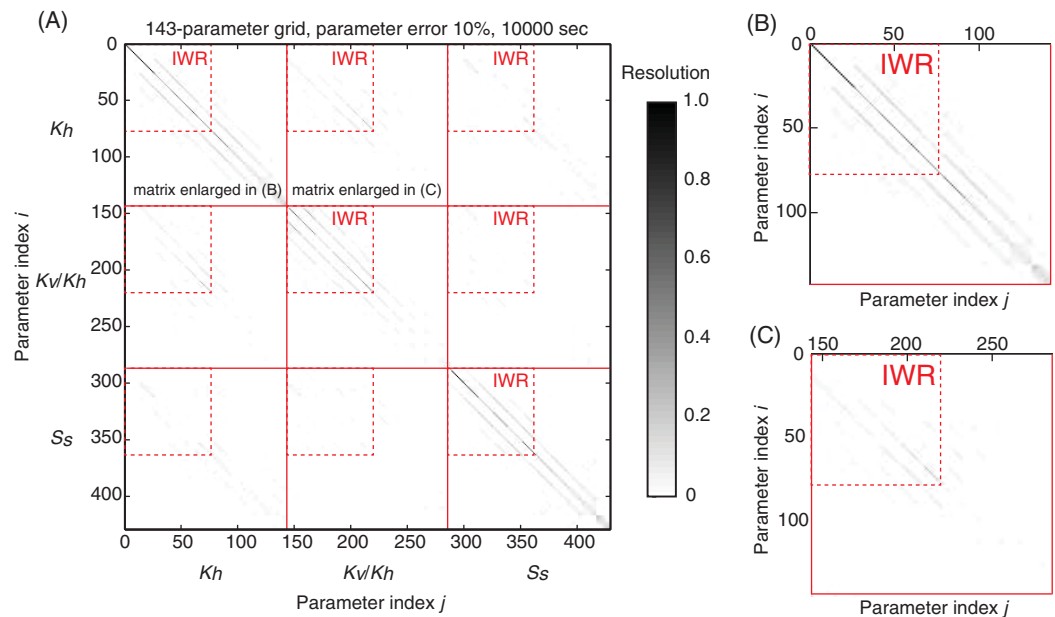


Figure 3. (a) Resolution matrix associated with the analysis of the synthetic 10,000 s head records for the base case scenario based on a truncated SVD of the sensitivity matrix shown in Figure 2a (truncated SVD with parameter error 10% and noise standard deviation 2×10^{-4} m). Red plain lines superposed on the resolution matrix indicate the different submatrices corresponding to each hydraulic property and dashed red boxes encompass parameters within the interwell region (IWR). Resolution matrix enlarged for (b) the top left submatrix showing resolution for K_h , and (c) top center submatrix showing resolution between K_h and K_v/K_h .

$$RMS_j = \sqrt{\frac{1}{n} \sum_{i=1}^n \left(K_h \frac{dh_i}{dK_h} \right)^2} = \sqrt{\frac{1}{n} \sum_{i=1}^n \left(\frac{dh_i}{d \ln K_h} \right)^2} \quad (17)$$

and similarly for K_v/K_h and S_s . The summation is over the entire set of n simulated heads for all stressed and observation intervals, and for all times over the tests. The RMS normalized sensitivity is an integrated measure of the sensitivity that emphasizes the resolution potential associated with relative variation of the sensitivities for each parameter. Thus, larger RMS normalized sensitivities could show better resolution potential. Figures 2b–2d also show temporal evolution of sensitivities by plotting RMS normalized sensitivity using (17) for different times; thus giving snapshots of RMS normalized sensitivity at specific times.

As summarized by Figure 2a or specifically illustrated at different times by Figures 2b–2d, Figures 2a–2d show that sensitivities are larger for cells near the stressed well, where flow rates induced by slug tests are the largest, with gradually decreasing values away from the stressed well as the head perturbation decays. Also, the comparison of sensitivity patterns along the study plane for each hydraulic property shows that sensitivities are larger for K_h with a radius of influence that extends well beyond the observation well. In comparison, sensitivities for K_v/K_h are relatively smaller and almost vanish just beyond the observation well. These patterns have to be related to the different flow components induced by slug tests, which induce predominantly horizontal head gradients even using a stressed screen of small aspect ratio (ratio of screen length to screen diameter). Sensitivities for S_s are the lowest and vary spatially according to temporal variation in head gradients. Thus, based solely on relative variation of sensitivities, the resolution potential is expected to be better for K_h near the stressed well.

3.1.2. Resolution Matrix and Resolution Tomograms

To further examine the potential of resolution of previous sensitivity plots presented in Figures 2a–2d, Figure 3a shows the resolution matrix associated to the same base case scenario. The computation of the elements of the resolution matrix is based on truncated SVD of the sensitivity matrix retaining the first 129 largest singular values and vectors, which corresponds to a relative parameter error of 10%. The resolution matrix is 439×439 , with top left, center, and bottom right 143×143 matrices associated with the K_h , K_v/K_h , and S_s values of the 143 parameter grid, respectively. The top middle, top right, and middle right matrices and their corresponding middle left, bottom left, and bottom middle mirror image matrices describe dependence

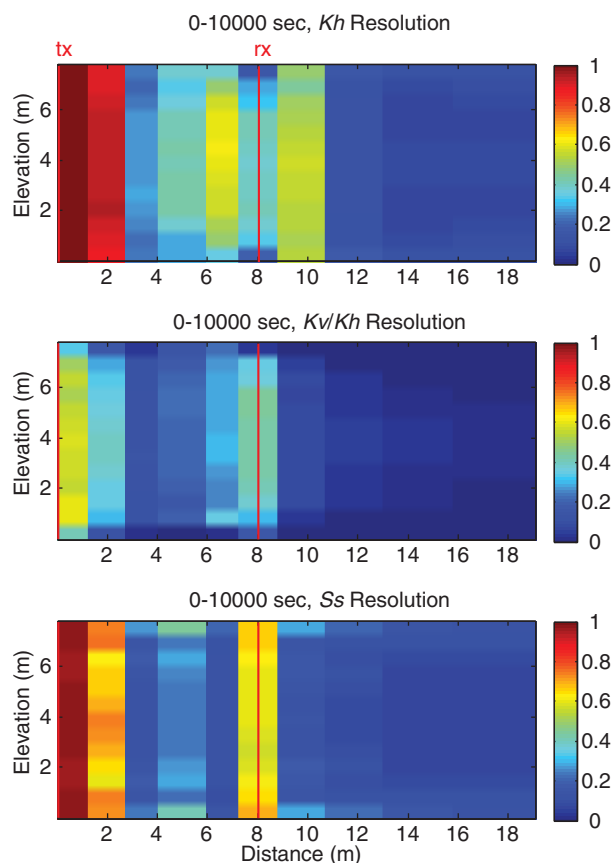


Figure 4. Diagonal elements of the resolution matrix (Figure 3a) for K_h , K_v/K_h , and S_s associated with the analysis of the synthetic 10,000 s head records for the base case scenario using an homogeneous and anisotropic model. The resolution values are based on a truncated singular value decomposition (SVD) of the sensitivity matrix for a relative parameter error of 10% and a random noise with a standard deviation of 2×10^{-4} m.

matrix in Figure 3a with darker diagonal elements, resolution values for K_h , K_v/K_h , and S_s are higher within the IWR and mostly focused on the stressed and observations wells with better resolution near the stressed well. For the central area within the IWR, the resolution is weak, as revealed by examination of Figure 3a that shows small resolution values spread along off-diagonal stripes running parallel to the diagonal, suggesting a correlation between these parameters and parameters on the diagonal. As noted in Table 1, average resolution values for K_h , K_v/K_h , and S_s within the IWR for the base case scenario range from 0.30 to 0.57.

3.1.3. Resolution Averaging Kernel

To complete the analysis of the resolution matrix with the base case scenario, Figures 5a–5c display averaging kernels associated with the inversion of K_h , K_v/K_h , and S_s for three cell locations in the 143 parameter grid (Figure 1b): cell 7 (Figure 5a) is located close to the stressed well, cell 46 (Figure 5b) is between the stressed and observation wells, and cell 98 (Figure 5c) is outside the IWR. As previously discussed with (14) and (15), every component of \mathbf{m}_i is a weighted average of the actual \mathbf{m} , with the weighting factors given by the elements of the resolution matrix \mathbf{R} . For this reason, the rows of \mathbf{R} are called averaging kernels and plotting the j resolution values of a given i th averaging kernel at corresponding locations in the investigated region provides information on the spatial averaging characteristics of the i th parameter [Vasco *et al.*, 1997]. That is, large spreading of resolution values in plotted averaging kernel around a i th parameter is indicative of coarse-scale spatial resolution, whereas resolution values centered on the given parameter reveal finer-scale resolution.

Note that for Figures 5a–5c, averaging kernels are extracted directly from the resolution matrix in Figure 3a. For the averaging kernel associated with cell 7 close to the stressed well in Figure 5a, an estimate of the hydraulic properties of this cell is essentially centered on the cell itself, except for K_v/K_h , where the kernel is

among the K_h , K_v/K_h , and S_s values. Each diagonal element of the 439×439 matrix describes the degree of resolution of the K_h , K_v/K_h , or S_s value in a particular model cell and ranges from 1 for a perfectly resolved parameter to 0 for a completely unresolved parameter. Off-diagonal elements of the resolution matrix describe the extent of blurring of a particular parameter estimate due to correlations with other parameters during the inversion process [Aster *et al.*, 2005]. Resolution values lower than 0.5 indicate that the parameter estimate for a cell is influenced more strongly by other parameter values than it is by the corresponding parameter of the cell itself. As illustrated in Figure 3a, while higher resolution values are essentially focused on the diagonal of the resolution matrix for cells within the IWR, nonzero resolution values also appear on off-diagonal elements. This suggests that parameters for the base case scenario are not perfectly resolved, and that correlation exists between cells for a given hydraulic property (e.g., Figure 3b) or between hydraulic properties for a given cell (e.g., Figure 3c).

To further illustrate the resolution information contained in the resolution matrix, Figure 4 shows the diagonal elements of the resolution matrix at the corresponding parameter grid cells for each hydraulic property. As expected from the resolution

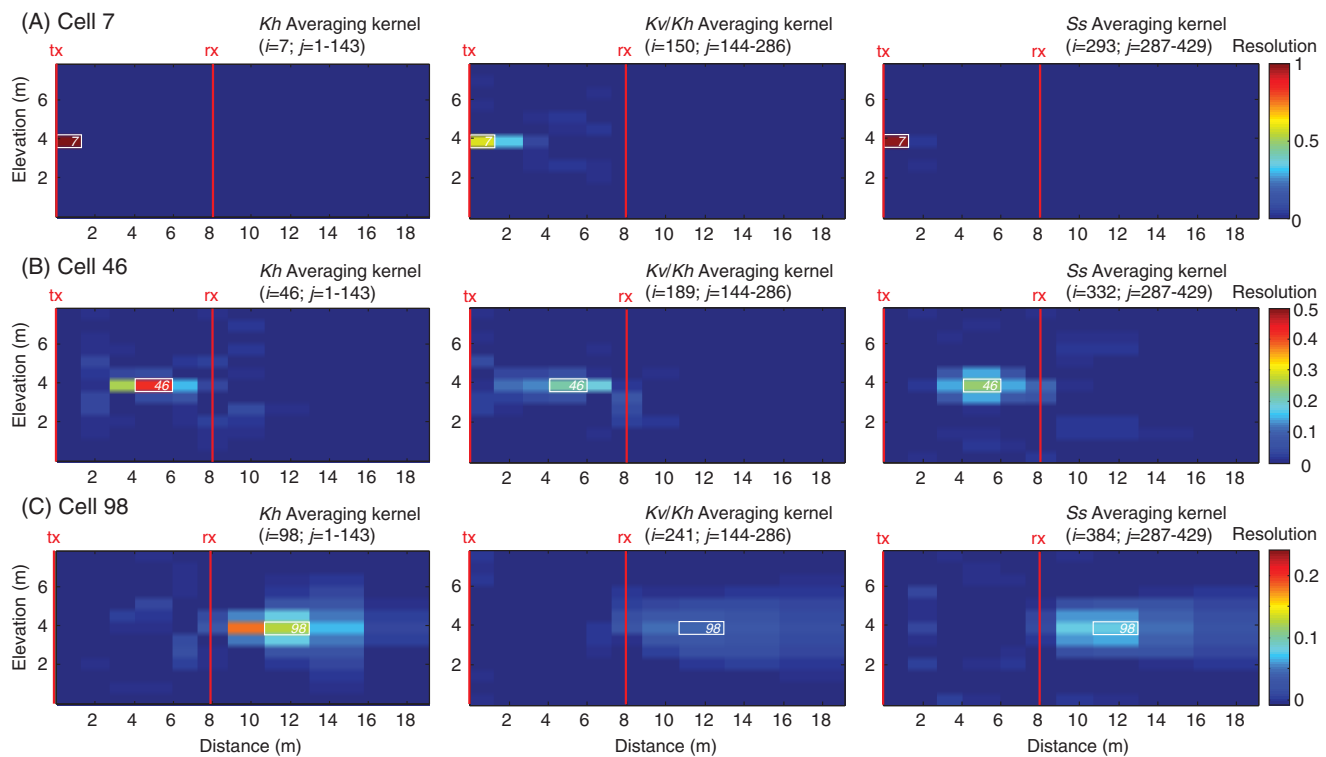


Figure 5. Averaging kernels (rows of the resolution matrix) extracted from the base case scenario resolution matrix depicted in Figure 3a for three selected cells: (a) cell 7 near the stressed well; (b) cell 46 in the middle of the interwell region (IWR); and (c) cell 98 outside the IWR. Indices i and j are row and column number of the resolution matrix in Figure 3a, respectively, which are associated with the plotted averaging kernel.

spreads over the two closest cells adjacent to the stressed well. In comparison, for estimates in the middle of the IWR (cell 46; Figure 5b), values for K_{hr} , K_v/K_{hr} , and S_s are averages over an approximately elliptical zone between the wells, whereas for a cell located outside the IWR (cell 98; Figure 5c), the averages are over much larger areas. Note also the difference the scale of the resolution for the three cells shown in Figures 5a–5c. Figures 5a–5c indicating that hydraulic parameters obtained from the inversion of tomographic slug tests head data are better resolved near the stressed well. For regions away from the wells (middle and outside the IWR), the resolution is rather weak so that K_{hr} , K_v/K_{hr} , and S_s estimates represent coarse-scale spatial averages. This means that for each incompletely resolved cell ($R < 1$), only the combined effects of this cell with its surrounding cells can be effectively resolved because the sensitivities for those cells are correlated. Finally it is important to mention that analyzing resolution using smaller parameter cell dimensions (vertically or horizontally) would have produced similar averaging kernel patterns, but with smaller relative resolution values for each cell.

3.2. Analysis of Factors Affecting Resolution

This section explores the impact on hydraulic property resolution from tomographic slug tests of the following factors: signal-to-noise ratio, test configuration, and magnitude of the hydraulic property. For each scenario, the resolution of parameters within the IWR is calculated and compared to the base case experiment. Figures 5a and 6a show the resolution for the three hydraulic parameters for the 143 parameter grid for the base case, whereas Figures 6b–6e and Figures 7b–7e show the same information for scenarios assessing the effects of different factors by comparison to the base case. As for the base case scenario, the resolution calculation is based on truncated SVD of the sensitivity matrix for a relative parameter error of 10% using an estimated random noise with a standard deviation of 2×10^{-4} m.

3.2.1. Effect of Signal-to-Noise Ratio

The relative magnitude of the sensitivity for a particular parameter or the sensitivity differences between given parameters compared to the measurement error (signal-to-noise ratio) is a critical consideration for parameter resolution [Yeh and Liu, 2000, Illman et al., 2008; Xiang et al., 2009; Huang et al., 2011; Liu and

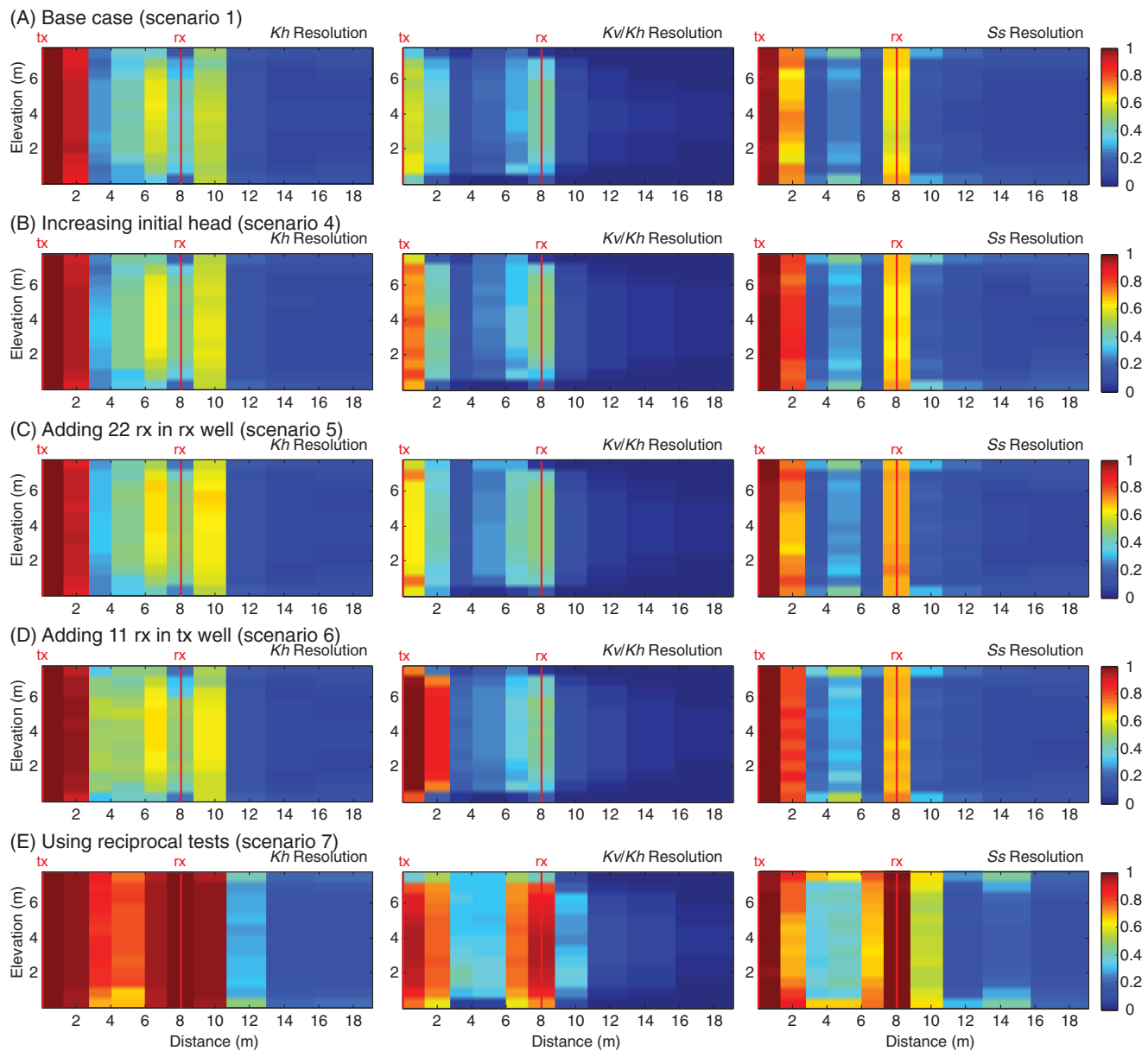


Figure 6. Diagonal elements of the resolution matrix for K_h , K_v/K_h , and S_s associated with the analysis of the synthetic 10,000 s head records (truncated SVD with parameter error 10% and noise standard deviation 2×10^{-4} m) for selected scenarios showing the effects of the signal-to-noise ratio and test configuration (Table 1): (a) base case with initial head of 4.5 m; (b) increasing initial head to 9.0 m; (c) adding 22 observation intervals in the observation well; (d) adding 11 observation intervals in the stressed well; and (e) using reciprocal tests.

Kitanidis, 2011]. For a small signal-to-noise ratio, it is indeed difficult to separate the real signal from the noise caused by measurement errors and then obtain reliable parameter estimates. Although the noise level is dependent on the technology available to record head data, the signal-to-noise ratio can be improved by increasing the magnitude of the head of the slug used to initiate tests. Figure 6b and Table 1 show indeed that doubling initial head from 4.5 to 9.0 m (scenario 4) slightly improves average resolution for K_h , K_v/K_h , and S_s within the IWR. However, comparing average resolutions for scenarios 1, 3, and 4 in Table 1 shows that the increase in resolution is reduced with increasing initial head (e.g. from 0.51 to 0.57 to 0.60 for K_h). This suggests that when head variations recorded in observation intervals are large enough to be no longer hindered by the noise, the resolution potential is then essentially controlled by sensitivity differences between parameters that are too small to be distinguished from the noise, such as for parameters in the middle and outside of the IWR. As an extreme example, when considering unrealistic noise-free head data

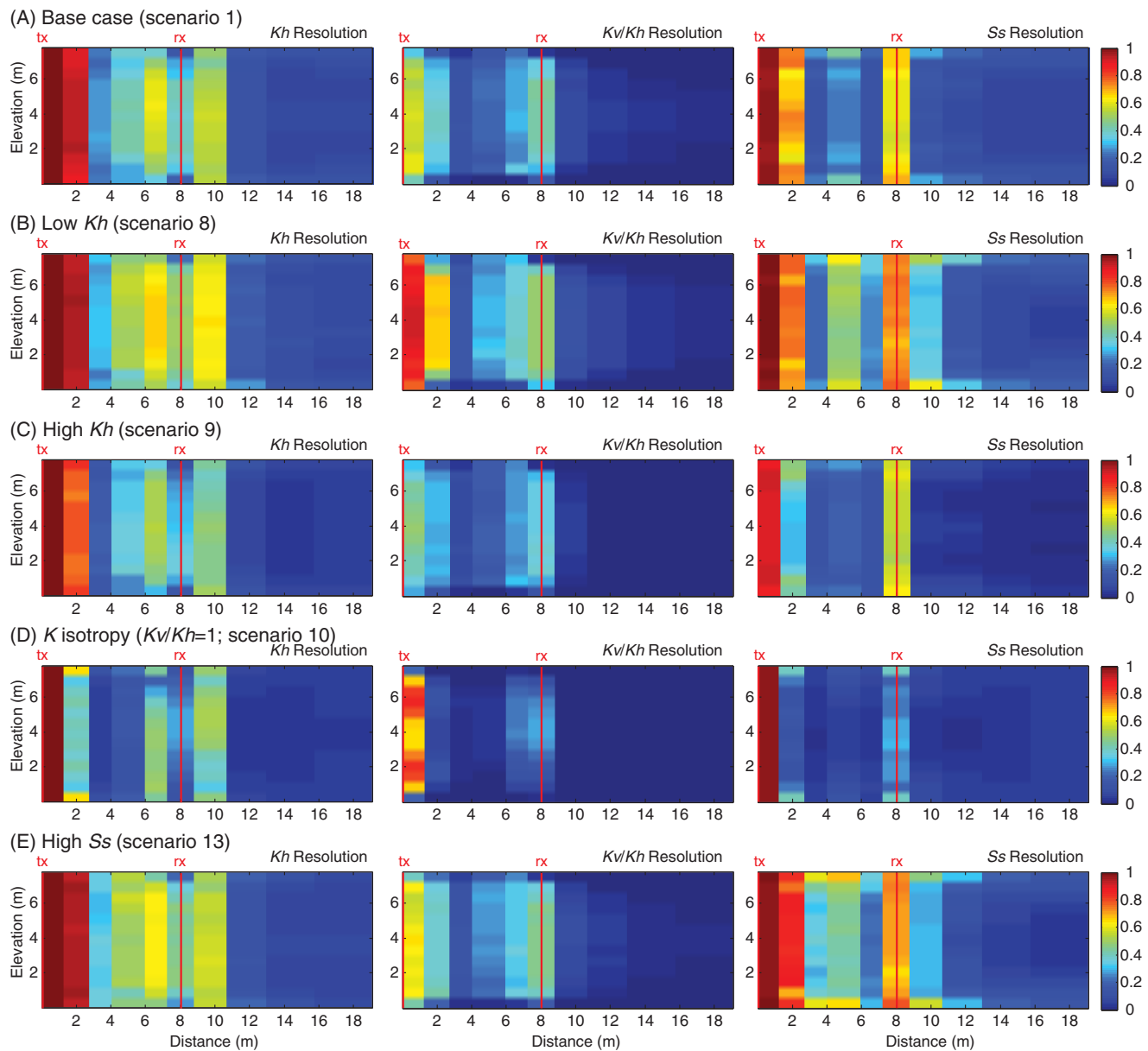


Figure 7. Diagonal elements of the resolution matrix for K_h , K_v/K_h , and S_s associated with the analysis of the synthetic 10,000 s head records (truncated SVD with parameter error 10% and noise standard deviation 2×10^{-4} m) for selected scenarios showing the effects of the magnitude of hydraulic property values (Table 1): (a) base case with K_h value of 1×10^{-5} m/s, K_v/K_h value of 0.1, and S_s value of 1×10^{-5} m⁻¹; (b) low K_h value of 1×10^{-6} m/s; (c) high K_h value of 1×10^{-4} m/s; (d) K isotropy with a K_v/K_h value of 1; and (e) high S_s value of 1×10^{-4} m⁻¹.

(scenario 2) for the base case scenario, Table 1 shows that small differences in sensitivity between parameters can easily be distinguished, which results in perfectly resolved parameters within the entire IWR.

3.2.2. Effect of Test Configuration

The number and relative location of observation intervals used to record head data during a tomographic experiment may affect hydraulic property resolution. As a reminder, the base case (scenario 1 in Table 1) used 3 observation intervals for each of the 13 test intervals (except at the top and base) for a total of 37 observation intervals (Figure 1b). To illustrate the effect of test configuration on resolution, three different scenarios are considered (Table 1): (scenario 5) the base case using 5 observation intervals per test instead of 3, for a total of 13 stressed and 59 observation interval responses; (scenario 6) the base case using one additional observation interval per test below the stressed interval (this configuration is identical to the

vertical interference slug tests proposed by *Paradis and Lefebvre*, [2013]), for a total of 13 stressed interval responses and 48 observation interval responses (37 in the observation well and 11 in the stressed well); and (scenario 7) the base case with its reciprocal mirror image where roles of stressed and observation wells are interchanged, for a total of 26 stressed and 74 observation interval responses.

Figure 6c and Table 1 show that using 22 additional observation intervals located in the observation well (scenario 5) slightly increases average resolution within the IWR with respect to the base case scenario. The comparison of Figures 6c and 6d indicates, however, that using additional observation intervals located in the stressed well (scenario 6), instead of in the observation well (scenario 5), provides better resolutions (Table 1), in particular for K_v/K_h , near the stressed well, even if fewer observation intervals are used. Indeed, an additional observation interval located at proximity to the source provides more information than an additional interval located close to an existing observation interval in the observation well. Notice that for practical situations dealing with heterogeneous aquifers, using many (and possibly close) observation intervals in an observation well may provide less redundant information than for the homogeneous case illustrated in the present paper.

As depicted in Figure 6e, using the base case with its reciprocal mirror image (scenario 7) considerably increases the resolution within the IWR (Table 1). For that case, reciprocal tests greatly contribute to reduce sensitivity correlation between parameters due to the distinct sensitivity behavior for stressed and observation interval responses [*McElwee et al.*, 1995]. This may appear contradictory to the finding of *Bohling and Butler* [2010] with respect to the benefit of using reciprocal tests. In their discussion regarding tomographic pumping tests, *Bohling and Butler* [2010] assume that when using observation interval responses, adding reciprocal observation interval responses do not indeed provide additional information about heterogeneities, as long as the principle of reciprocity [*Bruggeman*, 1972; *Leven and Dietrich*, 2006] holds. In our analysis, however, we used both stressed and observation interval responses, which together provide different information about heterogeneities regardless of the applicability of the principle of reciprocity. Obviously, using reciprocal tests requires twice the acquisition time in the field and may considerably increase the computational burden, but the major improvement in resolution compared to other experimental strategies has to be considered when planning the design of tomographic slug tests experiments.

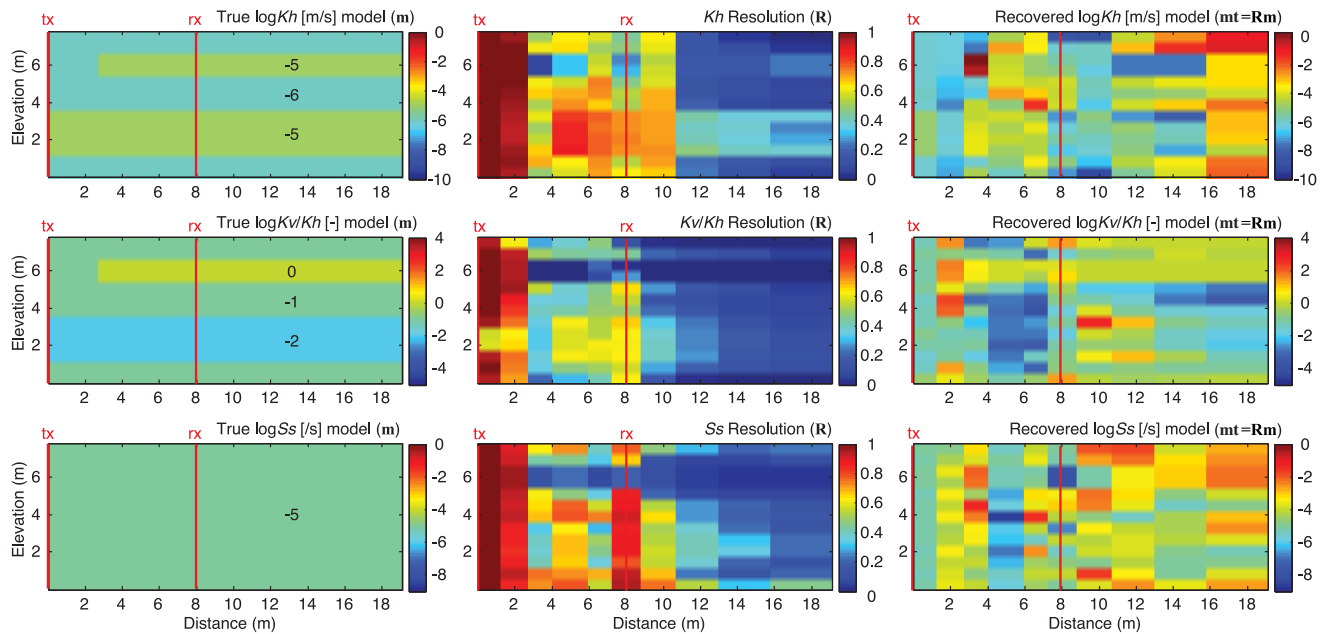
3.2.3. Effect of Magnitude of Hydraulic Property Values

The magnitude of hydraulic properties is expected to control the resolution potential of tomographic slug tests due to variations in both sensitivity magnitude and relative correlation between parameters that can be induced by different combinations of hydraulic property values. Figures 7b–7e and Table 1 (scenarios 8–13) present resolution tomograms and average resolutions within the IWR, respectively, for different combinations of K_h , K_v/K_h , and S_s . For each scenario, one hydraulic property is varied at a time while holding the other properties constant. By comparison with the base case scenario, we observe that resolution is better for a lower K_h value (scenario 8 versus 9), stronger K anisotropy (lower K_v/K_h) (scenario 10 versus 11), and a higher S_s value (scenario 12 versus 13). Changes in resolution are not only observed for the modified hydraulic property itself, but also together with the other properties in the same direction (all with better or worst resolution). Lower resolution for higher values of K_h and lower values of S_s (Table 1) is explained, in part, by the fact that faster head responses in observation intervals increase the correlation between sensitivities for stressed and observation intervals. Note, however, that a large S_s value leads to a smaller head response in the observation interval, which may limit proper resolution as the observation response should be larger than the noise level in the measurements. Lower resolution for isotropic conditions ($K_v/K_h = 1$) is on the other hand the result of almost identical head responses recorded in observation intervals with different angles with respect to the source, which is redundant information that cannot help distinguish the contribution of the different parameters. Indeed, for homogeneous and isotropic conditions, difference in travel path lengths with varying observation interval locations are not sufficient to produce significant difference in observation interval responses. In the field however, head responses recorded in observation intervals with different angles would inevitably exhibit differences as aquifers are rarely perfectly homogeneous and isotropic, and the analysis of head responses for various angles can help in identifying the degree of heterogeneity and/or anisotropy at the scale of the tomographic experiment.

3.3. Coarse-Scale Heterogeneities

Previous results demonstrated that resolution potential associated with hydraulic property values estimated from tomographic slug tests head data strongly varies spatially as a function of measurement error, test configuration, and magnitude in hydraulic property values. These results thus indicate the limitations of

(A) Fine spatial resolution (143-parameter grid)



(B) Coarse spatial resolution (65-parameter grid)

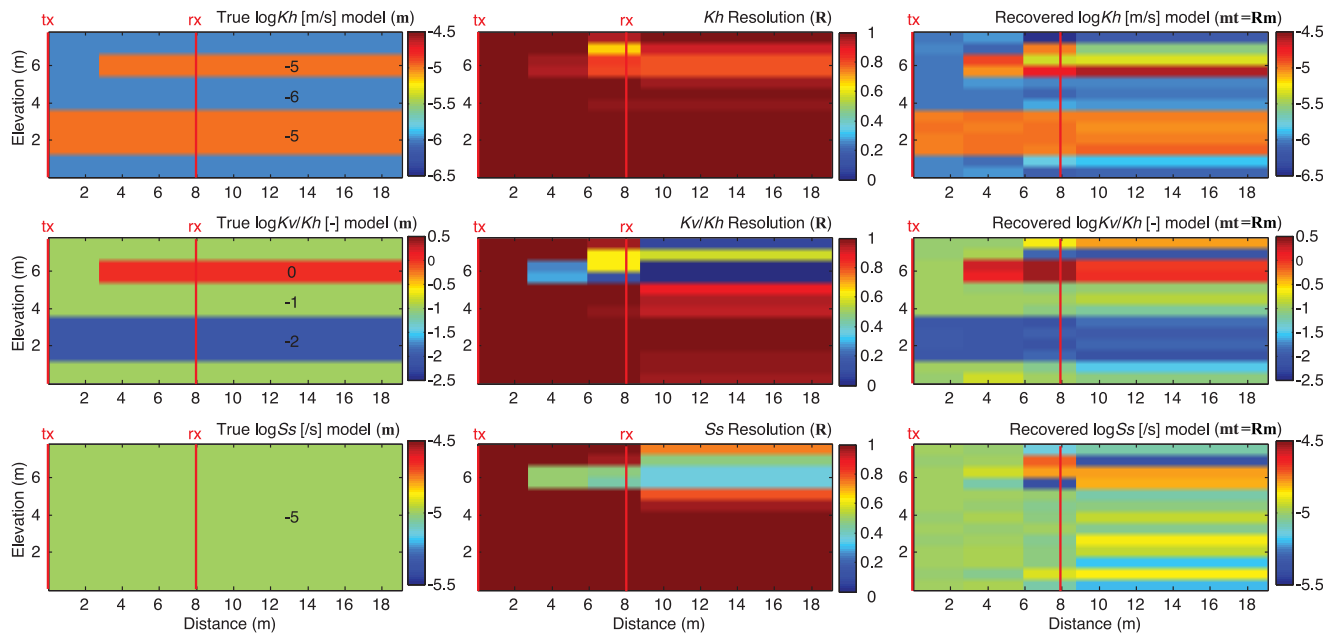


Figure 8. Recovered aquifer model for K_h , K_v/K_h , and S_s as obtained from the multiplication of the true heterogeneous model by the resolution matrix for a 10,000 s head records analysis (truncated SVD with parameter error 10% and noise standard deviation 2×10^{-4} m), showing the effects of the discretization of the parameter grid on heterogeneity resolution (Table 1): (a) fine spatial resolution with the 143 parameter grid shown in Figure 1b; and (b) coarse spatial resolution with a 65 parameter grid where cell dimensions were varied according to the approximate size of the averaging kernels of the 143 parameter grid.

such data to resolve by themselves (i.e., without regularization) fine-scale heterogeneities everywhere over the region investigated by slug tests. In this section, we evaluate the effect of model parameter grid discretization to define coarse-scale heterogeneity in hydraulic properties as contained in the averaging kernels. For that purpose, we consider an additional synthetic experiment using a heterogeneous model that mimics the general aquifer structure recovered from the inversion of the tomographic field experiment reported by *Paradis* [2014]. The main features of this model (Figures 8a and 8b) are: (i) a permeable ($K_h=1 \times 10^{-5}$ m/s) and strongly anisotropic ($K_v/K_h=0.01$) continuous layer in the lower part of the IWR; and (ii) a

permeable ($K_h=1 \times 10^{-5}$ m/s) and isotropic ($K_v/K_h=1$) discontinuous layer in the upper part of the IWR; (iii) that are embedded in lower permeability ($K_h=1 \times 10^{-6}$ m/s), and mild K anisotropy ($K_v/K_h=0.1$) material. Specific storage was kept at a constant value of $1 \times 10^{-5} \text{ m}^{-1}$ over the entire model domain. For this experiment, we use the base case test configuration with 22 additional observation intervals in the observation well (same as scenario 5) and 11 in the stressed well (same as scenario 6) to represent a field acquisition strategy with significantly improved resolution as indicated by previous results for a homogeneous domain (Table 1).

First, we consider the resolution and associated hydraulic property tomograms using the 143 parameter grid to assess recovery of the heterogeneities (Figure 8a). The recovered tomogram for K_h , K_v/K_h , and S_s are evaluated using (14) and (15), where the elements of the resolution matrix are the averaging coefficients resulting from the inversion. As expected from previous analysis with homogeneous and anisotropic models, the resolution is generally focused near the stressed and observation wells, even though resolution can be modified locally due to the difference in hydraulic property values. Consequently, recovered hydraulic properties from inversion are only similar to the true model near the stressed well and the true aquifer structure is hardly distinguishable from recovered tomograms due to the relatively poor resolution in the middle and outside of the IWR (Table 1). We also note the large variance of hydraulic property estimates (large deviation from the true average value), as indicated by the range of hydraulic property values on respective scale bars.

As illustrated in Figures 5a–5c, model parameter estimates are weighted averages of the true model parameters in the vicinity of the incompletely resolved cells, which means that an inversion can be regularized through discretization to lower sensitivity correlation, and provide parameter estimates with higher resolution [Aster *et al.*, 2005]. Reducing the number of cells between the stressed and observation wells can also achieve regularization through discretization. Figure 8b shows the resolution and recovered models for K_h , K_v/K_h , and S_s using a coarse 65 parameter grid. According to the averaging kernels of the previous simulation with the heterogeneous model, cells of the 143 parameter grid were merged together to separate the interior and exterior of the IWR in three and two columns of cell, respectively. For this example, cells within the IWR are thus 0.61×2.92 m (on average), whereas cells just beyond and farther away the observation well are 0.61×10.38 m and 0.61×91.70 m, respectively. According to Figure 8b and Table 1, the heterogeneous model is better resolved using a coarser parameter grid adapted to the scale of the information contained in the resolution matrix, thus providing a recovered model closer to the true model with smaller deviation from the true average hydraulic property values (note that different ranges of values were used on parameter scale bars in Figures 8a and 8b).

A few additional comments can be made about Figure 8b. First, merging cells of the discontinuous layer would have provided a better resolution of this layer, as well as using different discretization grids for each hydraulic property, as indicated by an analysis of the averaging kernels (not shown). Also, while magnitude in hydraulic property values have an influence on resolution potential, as shown for the discontinuous layer, the relative magnitude in hydraulic property values also appears to have an influence on resolution, as suggested by the low-resolution values for parameters in the top right corner of the IWR. While this issue is not formally addressed in this paper, the effects of relative magnitude in hydraulic property values could be related to test configuration, as the high permeability discontinuous layer seems to hide hydraulic responses in observation intervals located in the top right corner of the IWR. For instance, Scenario 16 in Table 1 shows that inverting the locations of stressed and observation intervals, where the discontinuous layer is now in direct contact with stressed intervals almost completely resolves this layer using the 65 parameter grid (not shown). This is expressed in Table 1 by average resolutions within the IWR that are over 0.95 for all hydraulic properties.

4. Discussion and Conclusions

This study examined the information content of tomographic slug tests head data for characterizing K_h , K_v/K_h , and S_s heterogeneities through a resolution analysis of synthetic scenarios based on the known characteristics of a littoral aquifer showing K anisotropy at different scales. The analysis uses a radial flow numerical model enabling the simulation of wellbore storage effects to represent hydraulic head propagation induced by slug tests in the plane encompassing stressed and observation wells. Resolution analysis was

carried out using truncated singular value decomposition of the sensitivity matrix, as a convenient way of analyzing least-squares inverse problems, in the absence of an explicit regularization term or a priori information, and using a noise level representative of field conditions. Various synthetic experiments were assessed to illustrate the effects of the signal-to-noise ratio, test configuration, magnitude in hydraulic properties, and discretization on the resolution potential of tomographic slug tests data. The main conclusions of this study can be stated as follows:

1. Governing groundwater flow equations that describe hydraulic head propagation from slug tests into aquifers appear a major limitation to resolution of hydraulic properties on the sole basis of head data. The resolution potential of tomographic slug tests for K_h , K_v/K_h , and S_s with a noise level representative of field conditions is indeed essentially focused on the stressed and observation wells as a result of correlation between parameters. That is, correlated parameters have similar effects on head variations and a small level of noise in the measurements can hinder their respective contributions. This is consistent with previous resolution analysis using tomographic pumping tests that share the same governing equations as slug tests [Vasco *et al.*, 1997; Clemo *et al.*, 2003; Bohling, 2009]. Thus, although head responses induced by multiple hydraulic tests are sensitive to hydraulic properties throughout the entire IWR and, to a lesser extent, at a fair distance away beyond the observation well, sensitivity magnitudes do not provide a sufficient condition to ensure proper resolution. Furthermore, correlations between parameters, which are exacerbated under noisy measurements, must be taken into account.
2. However, results also show that adequate test design can markedly improve the resolution potential, especially the choice of the initial head and the configuration of stressed and observation intervals. For instance, observation intervals located in the stressed well itself and the use of reciprocal tests can both greatly contribute to reduce sensitivity correlation between parameters. However, while vertical heterogeneities could be easily resolved using vertically closely spaced stressed and observation intervals, not much can be done in practice to considerably increase lateral resolution using head data alone, even with a dense network of stressed and observation intervals. Lateral resolution limitations could also be exacerbated for highly permeable and isotropic aquifers. Regularization of the inversion or conditioning to independent measures or indicators of hydraulic properties is thus required to obtain fine-resolution of representative hydraulic properties from tomographic slug tests experiments.
3. Although the diffuse nature of the resolution matrix associated with an analysis of tomographic head data limits the resolution of fine-scale heterogeneities, tomographic slug tests data are capable of providing key information about aquifers by independently resolving coarse-scale heterogeneities in K_h , K_v/K_h , and S_s . Averaging kernels, which provide averaging properties for each individual parameter of an inverse solution, indeed indicate that spatial resolution potential is space variable. Thus, fine-scale heterogeneities are better resolved near the wells, in particular near the stressed well, while coarse-scale heterogeneities could be resolved elsewhere within the IWR and even beyond the observation well over large areas. Results relative to the resolution potential outside the IWR are in accordance with Bohling [2009] that demonstrated that an analysis of tomographic pumping tests data is incapable of resolving fine-scale heterogeneities in K (assuming K isotropy) and S_s beyond the observation well (note that his analysis was for cells with dimensions 0.76×1.52 m), and with Sun *et al.*, [2013] that illustrated that tomographic depth-averaged pumping tests can depict heterogeneity patterns for transmissivity (T) and storativity (S) at low spatial resolution far away from the well field.
4. Still, an anisotropic framework for the analysis of tomographic slug tests data provides greater confidence in the estimated model parameters. This is particularly true for coarse-scale assessment of heterogeneities when fine-scale information about K anisotropy is not available, which may prove very useful at the preliminary stage of a characterization program or when the project objectives do not require finer investigations. Thus, even if the analysis shows that no anisotropy is required, one can have greater confidence in the isotropic model thus obtained if the analysis method is set in terms of an anisotropic framework [Babuska and Cara, 1991]. Then, as proposed in this study, fine-scale and coarse-scale K anisotropy effects can be captured using K_v/K_h values for the parameter grid cells and by resolving the heterogeneous structure of the aquifer, respectively.
5. Obviously, using a coarser discretization allows lower variance and a lower degree of parameter correlation for a more unique solution. However, this also induces bias, which is generally expressed by the

smoothing of the estimated parameters. This is a manifestation of the well-known bias-variance trade-off [Menke, 2012; Aster et al., 2005]. Thus, we are interested to find the optimum between resolution in parameter estimates and oversmoothing of the aquifer structures.

6. Moreover, as implied in our analysis of the resolution potential of tomographic slug tests head data, for fine-scale assessment of aquifer heterogeneities it is necessary to supply other fine-scale a priori information to reduce the bias that may be induced by a coarse discretization of an aquifer. This is especially important for regions in the middle of the IWR and beyond the observation well where the resolution potential is the lowest. This poses a challenge for field characterization and integration approaches aimed at finding appropriate a priori information to regularize tomographic inverse problems, because obtaining fine-scale information about K_h , K_v/K_h , and S_s is not simple in practice. This challenge is even greater in heterogeneous aquifers where hydraulic property distributions (e.g., mean, variance, spatial structure) may vary in relation with the various lithofacies present and be different for each hydraulic property. Overall, this study shows that as far as the information contained in tomographic slug tests head data is well-understood, the characterization of coarse-scale heterogeneity in K_h , K_v/K_h , and S_s could be an interesting alternative to conventional hydraulic methods in order to more precisely depict aquifer heterogeneities. A field-based application of tomographic slug tests using full head records will be the next logical step to further assess the potential of this characterization approach.
7. Finally, a caution should be mentioned here about the findings that are based on a radial flow model. Indeed, this study investigated the resolution for a two-dimensional wedge of an aquifer with a radial flow model, which does not perfectly translate to a fully three-dimensional analysis. In particular, the use of a two-dimensional radial flow model may artificially inflate the resolution compared to a three-dimensional case by restricting the head perturbation in two-dimensions instead of three-dimensions. For the resolution analysis presented in this paper, such a situation is obviously not a concern because simulated heterogeneities could be considered axis-symmetric, even if this conceptualization is not representative of field conditions. Under real field conditions, radially asymmetric heterogeneities may induce significant angular or lateral flux variations, and use of a radial flow model should be considered carefully in those cases because head responses measured in the plane between the stressed and observation wells can be biased.

Acknowledgments

This study was supported by the Geological Survey of Canada as part of the Groundwater Resources Inventory program, by the Régie intermunicipale de gestion des déchets des Chutes-de-la-Chaudière, and by NSERC Discovery Grants held by R.L. and E.G. This is ESS contribution number 20090447. Synthetic data used to produce the results of this paper are available upon request from the corresponding author. This paper benefited from the comments of G. C. Bohling, five anonymous reviewers, and one anonymous Associate Editor. Authors would also like to sincerely thank Alberto Montanari (Editor in Chief) who fairly managed the review of this manuscript.

References

- Anderson, M. P. (1989), Hydrogeologic facies models to delineate large-scale spatial trends in glacial and glaciofluvial sediments, *Geol. Soc. Am. Bull.*, *101*, 501–511.
- Aster, R. C., B. Borchers, and C. H. Thurber (2005), *Parameter Estimation and Inverse Problems*, 301 pp., Elsevier, Amsterdam, Netherlands.
- Babuska, V., and M. Cara (1991), *Seismic Anisotropy in the Earth*, 217 pp. Kluwer Acad., Boston, Mass.
- Bayer, P., P. Huggenberger, P. Renard, and A. Comunian (2011), Three-dimensional high resolution fluvio-glacial aquifer analog: Part 1: Field study, *J. Hydrol.*, *405*(1–2), 1–9, doi:10.1016/j.jhydrol.2011.03.038.
- Berg, S. J., and W. A. Illman (2011), Three-dimensional transient hydraulic tomography in a highly heterogeneous glaciofluvial aquifer-aquitard system, *Water Resour. Res.*, *47*, W10507, doi:10.1029/2011WR010616.
- Berg, S. J., and W. A. Illman (2013), Field study of subsurface heterogeneity with steady state hydraulic tomography, *Groundwater*, *51*(1), 29–40, doi:10.1111/j.1745-6584.2012.00914.x.
- Berg, S. J., and W. A. Illman (2015), Comparison of hydraulic tomography with traditional methods at a highly heterogeneous site, *Groundwater*, *53*(1), 71–89, doi:10.1111/gwat.12159.
- Bohling, G. C. (2009), Sensitivity and resolution of tomographic pumping tests in an alluvial aquifer, *Water Resour. Res.*, *45*, W02420, doi:10.1029/2008WR007249.
- Bohling, G. C., and J. J. Butler Jr. (2001), Lr2dinv: A finite-difference model for inverse analysis of two-dimensional linear or radial groundwater flow, *Comput. Geosci.*, *27*, 1147–1156.
- Bohling, G. C., and J. J. Butler Jr. (2010), Inherent limitations of hydraulic tomography, *Ground Water*, *48*, 809–824, doi:10.1111/j.1745-6584.2010.00757.x.
- Bohling, G. C., X. Zhan, J. J. Butler Jr., and L. Zheng (2002), Steady shape analysis of tomographic pumping tests for characterization of aquifer heterogeneities, *Water Resour. Res.*, *38*(12), 1324, doi:10.1029/2001WR001176.
- Bohling, G. C., J. J. Butler Jr., X. Zhan, and M. D. Knoll (2007), A field assessment of the value of steady-shape hydraulic tomography for characterization of aquifer heterogeneities, *Water Resour. Res.*, *43*, W05430, doi:10.1029/2006WR004932.
- Bolduc, A. (2003), Géologie des formations superficielles, Charny, Québec, Comm. Géol. du Canada, Dossier public 1976, échelle 1/50000.
- Bouwer, H., and R. C. Rice (1976), A slug test method for determining hydraulic conductivity of unconfined aquifers with completely or partially penetrating wells, *Water Resour. Res.*, *12*(3), 423–428.
- Brauchler, R., R. Liedl, and P. Dietrich (2003), A travel time based hydraulic tomographic approach, *Water Resour. Res.*, *39*(12), 1370, doi:10.1029/2003WR002262.
- Brauchler, R., J. Cheng, M. Everette, B. Johnson, P. Dietrich, R. Liedl, and M. Sauter (2007), An inversion strategy for hydraulic tomography: Coupling travel time and amplitude inversion, *J. Hydrol.*, *345*, 184–198, doi:10.1016/j.jhydrol.2007.08.011.

- Brauchler, R., R. Hu, T. Vogt, D. Halbouni, T. Heinrichs, T. Ptak, and M. Sauter (2010), Cross-well slug interference tests: An effective characterization method for resolving aquifer heterogeneity, *J. Hydrol.*, *384*, 33–45, 10.1016/j.jhydrol.2010.01.004.
- Brauchler, R., R. Hu, P. Dietrich, and M. Sauter (2011), A field assessment of high-resolution aquifer characterization based on hydraulic travel time and hydraulic attenuation tomography, *Water Resour. Res.*, *47*, W03503, doi:10.1029/2010WR009635.
- Bruggeman, G. A. (1972), The reciprocity principle in flow through heterogeneous porous media, in *Fundamentals of Transport Phenomena in Porous Media*, edited by International Association for Hydraulic Research (IAHR), pp. 136–149, Elsevier, Amsterdam, Netherlands.
- Butler, Jr., J. J., and C. D. McElwee (1995), Well-testing methodology for characterizing heterogeneities in alluvial-aquifer systems: Final technical report, Kans. Geol. Surv. Open File Report no. 75–95.
- Butler, J. J., Jr., C. D. McElwee, and G. C. Bohling (1999), Pumping tests in networks of multilevel sampling wells: Motivation and methodology, *Water Resour. Res.*, *35*(11), 3553–3560, doi:10.1029/1999WR900231.
- Caers, J. (2005), *Petroleum Geostatistics*, 88 pp., Soc. of Pet. Eng., Richardson, Tex.
- Cardiff, M., and W. Barrash (2011), 3-D transient hydraulic tomography in unconfined aquifers with fast drainage response, *Water Resour. Res.*, *47*, W12518, doi:10.1029/2010WR010367.
- Cardiff, M., W. Barrash, P. K. Kitanidis, B. Malama, A. Revil, S. Straface, and E. Rizzo (2009), A potential-based inversion of unconfined steady-state hydraulic tomography, *Ground Water*, *47*(2), 259–270, doi:10.1111/j.1745-6584.2008.00541.x.
- Cardiff, M., W. Barrash, and P. K. Kitanidis (2012), A field proof-of-concept of aquifer imaging using 3-D transient hydraulic tomography with modular, temporarily-emplaced equipment, *Water Resour. Res.*, *48*, W05531, doi:10.1029/2011WR011704.
- Carrera, J., and S. P. Neuman (1986), Estimation of aquifer parameters under transient and steady state conditions: 1. Maximum likelihood method incorporating prior information, *Water Resour. Res.*, *22*(2), 199–210, doi:10.1029/WR022i002p00199.
- Carrera, J., A. Alcolea, A. Medina, J. Hidalgo, and L. J. Slouten (2005), Inverse problem in hydrogeology, *Hydrogeol. J.*, *13*, 206–222, doi:10.1007/s10040-004-0404-7.
- Chen, X., H. Murakami, M. S. Hahn, G. E. Hammond, M. L. Rockhold, J. M. Zachara, and Y. Rubin (2012), Three-dimensional Bayesian geostatistical aquifer characterization at the Hanford 300 Area using tracer test data, *Water Resour. Res.*, *48*, W06501, doi:10.1029/2011WR010675.
- Clemo, T., P. Michaels, and R. M. Lehman (2003), Transmissivity resolution obtained from the inversion of transient and pseudo-steady drawdown measurements, in *Proceedings of MODFLOW and More 2003 Understanding Through Modeling*, pp. 629–633, Int. Ground Water Model. Cent., Golden Colo.
- Cooper, H. H., Jr., J. D. Bredehoeft, and I. S. Papadopoulos (1967), Response of a finite diameter well to an instantaneous charge of water, *Water Resour. Res.*, *3*(1), 263–269, doi:10.1029/WR003i001p00263.
- Day-Lewis, F. D., K. Singha, and A. M. Binley (2005), Applying petrophysical models to radar travel time and electrical resistivity tomograms: Resolution-dependent limitations, *J. Geophys. Res.*, *110*, B08206, doi:10.1029/2004JB003569.
- Di Maio R., S. Fabbrocino, G. Forte, and E. Piegari (2014), A three-dimensional hydrogeological-geophysical model of a multi-layered aquifer in the coastal alluvial plain of Sarno River (southern Italy), *Hydrogeol. J.*, *22*, 691–703, doi:10.1007/s10040-013-1087-8.
- Doherty, J. (2003), Ground water model calibration using pilot points and regularization, *Ground Water*, *41*(2), 170–177, doi:10.1111/j.1745-6584.2003.tb02580.x.
- Fiene, M. N., T. Clemo, and P. K. Kitanidis (2008), An interactive Bayesian geostatistical inverse protocol for hydraulic tomography, *Water Resour. Res.*, *44*, W00B01, doi:10.1029/2007WR006730.
- Gottlieb, J., and P. Dietrich (1995), Identification of the permeability distribution in soil by hydraulic tomography, *Inverse Probl.*, *11*, 353–360, doi:10.1088/0266-5611/11/2/005.
- Hu, R., R. Brauchler, M. Herold, P. Bayer (2011), Hydraulic tomography analog outcrop study: Combining travel time and steady shape inversion, *J. Hydrol.*, *409*(1–2), 350–362, doi:10.1016/j.jhydrol.2011.08.031.
- Huang, S.-Y., J.-C. Wen, T.-C. J. Yeh, W. Lu, H.-L. Juan, C.-M. Tseng, J.-H. Lee, and K.-C. Chang (2011), Robustness of joint interpretation of sequential pumping tests: Numerical and field experiments, *Water Resour. Res.*, *47*, W10530, doi:10.1029/2011WR010698.
- Illman, W. A., X. Liu, and A. Craig (2007), Steady-state hydraulic tomography in a laboratory aquifer with deterministic heterogeneity: Multi-method and multiscale validation of hydraulic conductivity tomograms, *J. Hydrol.*, *341*(3–4), 222–234, doi:10.1016/j.jhydrol.2007.05.011.
- Illman, W.A., A.J. Craig, and X. Liu (2008), Practical issues in imaging hydraulic conductivity through hydraulic tomography, *Ground Water*, *46*(1), 120–132, doi:10.1111/j.1745-6584.2007.00374.x.
- Illman, W. A., X. Liu, S. Takeuchi, T. J. Yeh, K. Ando, and H. Saegusa (2009), Hydraulic tomography in fractured granite: Mizunami underground research site, Japan, *Water Resour. Res.*, *45*, W01406, doi:10.1029/2007WR006715.
- Kitanidis, P. K. (1995), Quasi-linear geostatistical theory for inverting, *Water Resour. Res.*, *31*(10), 2411–2419.
- Leven, C., and P. Dietrich (2006), What information we get from pumping tests? Comparing pumping configurations using sensitivity coefficients, *J. Hydrol.*, *319*, 199–215.
- Liu, X., and P. K. Kitanidis (2011), Large-scale inverse modeling with an application in hydraulic tomography, *Water Resour. Res.*, *47*, W02501, doi:10.1029/2010WR009144.
- McElwee, C.D., J. J. Butler Jr., and G. C. Bohling (1995), Sensitivity analysis of slug tests II: Observation wells, *J. Hydrol.*, *164*, 69–87.
- Menke, W. (2012), *Geophysical Data Analysis: Discrete Inverse Theory*, 3rd ed., 293 pp., Academic Press, Elsevier.
- Moore, E. H. (1920), On the reciprocal of the general algebraic matrix, *Bull. Am. Math. Soc.*, *26*, 394–395.
- Ouillon T., R. Lefebvre, D. Marcotte, A. Boutin, V. Blais, and M. Parent (2008), Hydraulic conductivity heterogeneity of a local deltaic aquifer system from the kriged 3D distribution of hydrofacies from borehole logs, Valcatier, Canada, *J. Hydrol.*, *351*(1–2), 71–86.
- Paradis, D. (2014), Contributions au développement de la caractérisation de l'hétérogénéité hydraulique des aquifères, Thèse de doctorat, 290 p., Univ. du Québec, Cent. Eau Terre Environ. [Available at <http://espace.inrs.ca/id/eprint/2307>.]
- Paradis, D., and R. Lefebvre (2013), Single-well interference slug tests to assess the vertical hydraulic conductivity of unconsolidated aquifers, *J. Hydrol.*, *478*(25), 102–118, doi:10.1016/j.jhydrol.2012.11.047.
- Paradis, D., R. Lefebvre, R. H. Morin, and E. Gloaguen (2011), Permeability profiles in granular aquifers using flowmeters in direct-push wells, *Ground Water*, *49*, 534–547, doi:10.1111/j.1745-6584.2010.00761.x.
- Paradis, D., L. Tremblay, R. Lefebvre, E. Gloaguen, A. Rivera, M. Parent, J.-M. Ballard, Y. Michaud, and P. Brunet (2014), Field characterization and data integration to define the hydraulic heterogeneity of a shallow granular aquifer at a sub-watershed scale, *Environ. Earth Sci.*, *72*(5), 1325–1348, Quebec, doi:10.1007/s12665-014-3318-2.
- Penrose, R. (1955), A generalized inverse for matrices, *Proc. Cambridge. Philos. Soc.*, *51*, 406–413.
- Prats, M., and J. B. Scott (1975), Effect of wellbore storage on pulse-test pressure response, *J. Pet. Technol.*, *27*, 707–709.
- Rubin, Y., and S. S. Hubbard (Eds.) (2005), *Hydrogeophysics*, 523 pp., Springer, Dordrecht, Netherlands.
- Sageev, A. (1986), Slug test analysis, *Water Resour. Res.*, *22*(8), 1323–1333.

- Soueid Ahmed, S. A., A. Jardani, A. Revil, and J. P. Dupont (2014), Hydraulic conductivity field characterization from the joint inversion of hydraulic heads and self-potential data, *Water Resour. Res.*, *50*, 3502–3522, doi:10.1002/2013WR014645.
- Spaine, F.A., Jr. (1996), Applicability of slug interference tests for hydraulic characterization of unconfined aquifers: (1) analytical assessment, *Ground Water*, *34*(1), 66–74.
- Sun, R., T.-C. J. Yeh, D. Mao, M. Jin, W. Lu, and Y. Hao (2013), A temporal sampling strategy for hydraulic tomography analysis, *Water Resour. Res.*, *49*, 3881–3896, doi:10.1002/wrcr.20337.
- Tikhonov, A. N. (1963), Regularization of incorrectly posed problems, *Sov. Math. Dokl.*, *4*(6), 1624–1627.
- Tikhonov, A. N., and V. A. Arsenin (1977), *Solution of Ill-Posed Problems*, 258 pp., John Wiley, N. Y.
- Tonkin, M. J., and J. Doherty (2005), A hybrid regularization methodology for highly parameterized environmental models, *Water Resour. Res.*, *41*, W10412, doi:10.1029/2005WR003995.
- Tosaka, H., K. Masumoto, and K. Kojima (1993), Hydropulse tomography for identifying 3-D permeability distribution in High Level Radioactive Waste Management, in *Proceedings of the Fourth Annual International Conference of the ASCE*, pp. 955–959, Am. Soc. Civ. Eng., Reston, Va.
- Tremblay, L., R. Lefebvre, D. Paradis, and E. Gloaguen (2014), Conceptual model of leachate migration in a granular aquifer from the integration of detailed characterization data, *Hydrogeol. J.*, *22*, 587–608, doi:10.1007/s10040-013-1065-1.
- Vasco, D. W., A. Datta-Gupta, and J. C. S. Long (1997), Resolution and uncertainty in hydrologic characterization, *Water Resour. Res.*, *33*(3), 379–397, doi:10.1029/96WR03301.
- Vogel, C. R. (2002), *Computational Methods for Inverse Problems*, 183 pp., Soc. for Ind. and Appl. Math., Philadelphia, Pa.
- Xiang, J., T.-C. J. Yeh, C.-H. Lee, K.-C. Hsu, and J.-C. Wen (2009), A simultaneous successive linear estimator and a guide for hydraulic tomography analysis, *Water Resour. Res.*, *45*, W02432, doi:10.1029/2008WR007180.
- Yeh, T.-C. J., and S. Liu (2000), Hydraulic tomography: Development of a new aquifer test method, *Water Resour. Res.*, *36*(8), 2095–2105, doi:10.1029/2000WR900114.
- Zha, Y., T.-C. J. Yeh, D. Mao, J. Yang, and W. Lu (2014), Usefulness of flux measurements during hydraulic tomographic survey for mapping hydraulic conductivity distribution in a fractured medium, *Adv. Water Resour.*, *71*, 162–176, doi:10.1016/j.advwatres.2014.06.008.
- Zhu, J., and T.-C. J. Yeh (2005), Characterization of aquifer heterogeneity using transient hydraulic tomography, *Water Resour. Res.*, *41*, W07028, doi:10.1029/2004WR003790.